Jurnal Kejuruteraan 38(5) 2026: 2277-2290
https://doi.org/10.17576/jkukm-2026-38(5)-15

Influence of c-CFRP Plate Length Variation on the Performance of Plain Concrete Beams under Four-Point Bending Test

Zaim Omar[a*], Swathika Murugesan[b], Sugiman Sugiman[c], Dianah Mazlan[a] & Hilton Ahmad[d*]

[a]*School of Civil Engineering, Tuanku Syed Sirajuddin Engineering Campus, Universiti Sains Malaysia, 14300 Nibong Tebal, Penang, Malaysia*

[b]*Department of Civil Engineering, KPR Institute of Engineering and Technology, Coimbatore, Tamil Nadu, India*

[c]*Faculty of Engineering, Department of Mechanical Engineering, University of Mataram, Mataram, Indonesia*

[d]*Department of Civil Engineering, Faculty of Civil Engineering and Built Environment, Universiti Tun Hussein Onn Malaysia, 86400, Parit Raja, Batu Pahat, Johor Darul Tak'zim, Malaysia*

**Corresponding author: cezaimom@usm.my & hilton@uthm.edu.my*

Received 4 December 2025, Received in revised form 26 March 2026
Accepted 26 April 2026, Available online 30 August 2026

ABSTRACT

The use of externally bonded carbon fibre-reinforced polymer (CFRP) plates for flexural strengthening of concrete beams has been well established; however, limited studies have explicitly focused on co-cured CFRP (c-CFRP) plates applied to plain concrete beams without internal reinforcement. Crack control and interface bonding become critical in such systems, yet the optimal c-CFRP plate length for effective stress transfer and energy absorption remains unclear. This study addresses this gap using a four-point bending test setup to investigate the flexural behaviour of plain concrete beams strengthened with two-layer c-CFRP plates of varying lengths (100 mm to 250 mm). The results show that increasing the plate length improves ultimate load, energy absorption, and deflection capacity. The 200 mm c-CFRP length achieved the most balanced performance, reaching an ultimate load of 15.61 kN and an energy absorption of 21.66 kN·mm. The 250 mm plate provided the highest overall capacity (18.94 kN) but exhibited signs of controlled delamination. In contrast, shorter plates led to shear cracks at the plate tip due to inadequate anchorage. These findings highlight the critical role of plate length in governing failure modes and stress distribution, offering practical guidance for optimising c-CFRP retrofit strategies. Future studies are recommended to investigate bond quality, multi-layer configurations, and environmental durability for long-term applications.

Keywords: Carbon fibre; polymer matrix composites (PMCs); stress concentration; flexural strengthened; joints/ joining

INTRODUCTION

Over the past two decades, the use of fibre-reinforced polymers (FRPs) for strengthening and retrofitting existing concrete structures has garnered considerable attention, particularly due to their high strength-to-weight ratio, corrosion resistance, and minimal alteration to the original structural geometry (Shrivastava & Tiwari, 2018). Among various FRP systems, carbon fibre-reinforced polymer (CFRP) has proven especially effective in enhancing the flexural performance of concrete elements. Externally bonded CFRP plates or sheets, when applied to the tension face of concrete members, have shown the potential to significantly improve load-carrying capacity, crack control, and stiffness under static and fatigue loading conditions (Tang et al. 2020). These improvements are especially valuable in structures that suffer from age-related degradation, poor construction practices, or increasing service demands (Obaidat et al. 2026).The comprehensive review by Ferreira et al. (2017) emphasises that the overall success of CFRP strengthening systems depends on material properties and critical parameters, including plate length, adhesive characteristics, surface preparation, and failure mode control. The interface between the CFRP and the concrete substrate determines the effectiveness of load transfer and the initiation of failure. Inadequate bond length or anchorage often leads to premature debonding, especially in beams without internal steel reinforcement. Several studies have investigated CFRP's bonding efficiency and stress transfer mechanisms in beam systems, highlighting the critical role of anchorage and interface properties (Gao et al. 2016; Kumar et al. 2020; Nadzri et al. 2020). For example, pre-stressed or self-anchored CFRP plates significantly enhanced load bearing and crack control in prestressed RC beams through improved stress redistribution and flexural stiffness (Vinh et al. 2022; Yazdani et al. 2020). Furthermore, strand-type and woven CFRP plates with advanced bonding characteristics demonstrated superior ductility and load capacity, especially when optimally positioned along the tensile face of beams (Yang et al. 2021).

Huang et al. (2015a) systematically examined the flexural performance of plain concrete beams externally strengthened with CFRP plates of varying lengths (100 mm, 200 mm, and 300 mm), focusing on understanding the influence of bonded length on load capacity, crack development, and failure behaviour. The results revealed that increasing the CFRP plate length significantly enhanced both the load-bearing capacity and flexural stiffness of the beams, with the 300 mm plate demonstrating the highest performance in energy absorption and delayed crack propagation. Shorter CFRP lengths, such as 100 mm, were insufficient to achieve full composite action and often led to premature failure, including debonding or shear cracking near the plate ends. Furthermore, the length of the CFRP plate is a key parameter influencing the performance of plain concrete beams, with longer plates improving ductility and reducing debonding issues (Al-Rousan et al. 2018). Recent advancements in experimental techniques, such as high-resolution crack tracking and staged failure analysis, have revealed that optimal CFRP application is not merely a function of material strength, but a balance between plate geometry, adhesive performance, and stress distribution (Kang et al. 2012; Maulana et al. 2022). Tiwary et al. (2022) and others have emphasised the importance of layout optimisation and pre-treatment strategies to delay delamination and failure.

In the traditional hand lay-up method, CFRP sheets are manually bonded to the surface of a cured concrete beam using a wet epoxy adhesive (Liao et al. 2026). This technique involves applying the resin to the CFRP and the concrete surface and curing at ambient or slightly elevated temperatures. In the study investigating mussel shell bio-filler epoxy adhesives for CFRP-strengthened concrete beams, CFRP plates of varying lengths (50 mm, 100 mm, 150 mm, 200 mm, and 250 mm) were bonded using a conventional hand lay-up method (Azhar et al. 2025). Among all configurations, the 250 mm plate achieved the highest peak force and ductility, followed by the 200 mm and 150 mm plates, confirming the critical influence of bonded length on effective stress transfer and crack bridging. Conversely, shorter plates, 50 mm and 100 mm, experienced a shear crack outside the bonding region due to the limited anchorage length. The dominant failure modes shifted from shear crack at short lengths to more ductile flexural behaviour in longer plates. Although the modified adhesive incorporating 7.5% mussel shell powder improved toughness, using a hand lay-up process remains sensitive to interface quality, especially at shorter lengths (Azhar et al. 2025). While it is widely used due to its simplicity and field applicability, hand lay-up is sensitive to several issues, including variability in adhesive thickness, incomplete wetting, air voids, and inconsistent bond quality, all of which can compromise the long-term performance and introduce premature debonding or delamination (Muravsky et al. 2025; Younas et al. 2026).

In contrast, c-CFRP involves pre-fabricating the CFRP laminate with the adhesive resin in a controlled environment, allowing both the fibre matrix and adhesive to cure simultaneously under pressure and elevated temperature (Motsch-Eichmann et al. 2021). This produces a uniformly consolidated composite plate with a homogeneous bond interface. When this co-cured laminate is bonded to the concrete surface using a thin epoxy layer (typical in hand lay-up), the risk of weak interfacial zones or resin-rich areas is significantly reduced (Zhou et al. 2025). Furthermore, the c-CFRP exhibits improved dimensional stability, higher surface quality, and stronger matrix integrity, collectively contributing to more effective stress transfer, crack control, and delay of failure modes such as delamination or shear crack propagation at the plate tip.

The co-curing technique has gained attention as a method to improve the bonding performance and structural integrity of CFRP joints. In recent studies, notably by Quan et al. (2022), co-curing was explored as an alternative to traditional secondary and co-bonding techniques. The co-curing process uses surface-treated Carbon Fibre/Polyether Ether Ketone (CF/PEEK) tapes instead of epoxy adhesives. This process enabled concurrent curing of composite adherends and bonding layers, significantly enhancing the joint's mechanical performance. Their findings showed substantial improvements, including up to a 68% increase in lap shear strength at elevated temperatures, and fracture energy improvements of 182% in Mode-I and 59% in Mode-II fracture tests. The enhanced performance was attributed to the plastic deformation of the PEEK matrix and extensive fibre bridging and delamination (Quan, Farooq, et al. 2022).

Thus, this study explores the flexural performance of plain concrete beams externally strengthened with two-layer c-CFRP plates of varying lengths (100 mm to 250 mm). Using a four-point bending test setup, a systematic evaluation of load-deflection responses, failure modes, crack propagation, and energy absorption characteristics. Through visual inspections and quantitative analysis, the influence of CFRP plate length on load transfer, failure transition, and stiffness is assessed. By identifying the optimal CFRP length that achieves effective crack control, delayed failure, and enhanced ductility, this work contributes toward refining design guidelines for FRP retrofitting in plain concrete applications. Noted that, plain concrete beams without internal reinforcement were selected to isolate and examine the direct contribution of c-CFRP plates as an external strengthening material. Excluding reinforcement bars ensured that the observed flexural behaviour, crack propagation, and failure characteristics were governed solely by the c-CFRP strengthening system, eliminating potential interactions with steel reinforcement. Although the effect of CFRP plate length on flexural performance has been widely studied, most investigations have relied on hand lay-up systems applied directly on concrete beams. Given this context, the current study addresses two significant gaps. First, there is no targeted investigation into c-CFRP plates with varied lengths applied to plain concrete. Second, there is limited understanding of the effects of c-CFRP length on the onset of cracking, ultimate load, energy absorption, and stiffness in the absence of internal rebar. This approach provides a fundamental understanding of the effectiveness of plate length, bond behaviour, and interface-controlled failure modes.

EXPERIMENTAL INVESTIGATION

This section focused on material preparation, which included the concrete beam, the c-CFRP plate, and the externally bonded plates on the concrete beam. The bending testing procedure was also described in this section.

TESTING SERIES

Figure 1 shows that the plain concrete beam's size was 400 x 100 x 100 mm³, with a clear span of 300 mm between supports, resulting in a span-to-depth (*L/d)* ratio of 3. On the other hand, the woven fabric carbon fibre (normal CFRP) with a double ply was used, with a nominal thickness of 0.166 mm and a density of 1.76 g/cm³. The density for epoxy resin is 1.16 g/cm³, which has been used to cure CFRP. During fabrication of c-CFRP, the width, W_f and thickness,t_f were controlled at 50 mm and 2 mm, respectively. Table 1 shows the designation for the control beam and the beams with varying CFRP plate lengths: CTL and L100, L150, L200 and L250, respectively. The cast specimen includes the control beam (without c-CFRP) and the strengthened beams with varying lengths,n L_f of c-CFRP. These CFRP plates were applied to the surface of the concrete beams at varying lengths of 100 mm, 150 mm, 200 mm, and 250 mm. Table 1 presents the dimensions, volume, volume fraction, number of specimens cast, and designation of the CFRP plates.

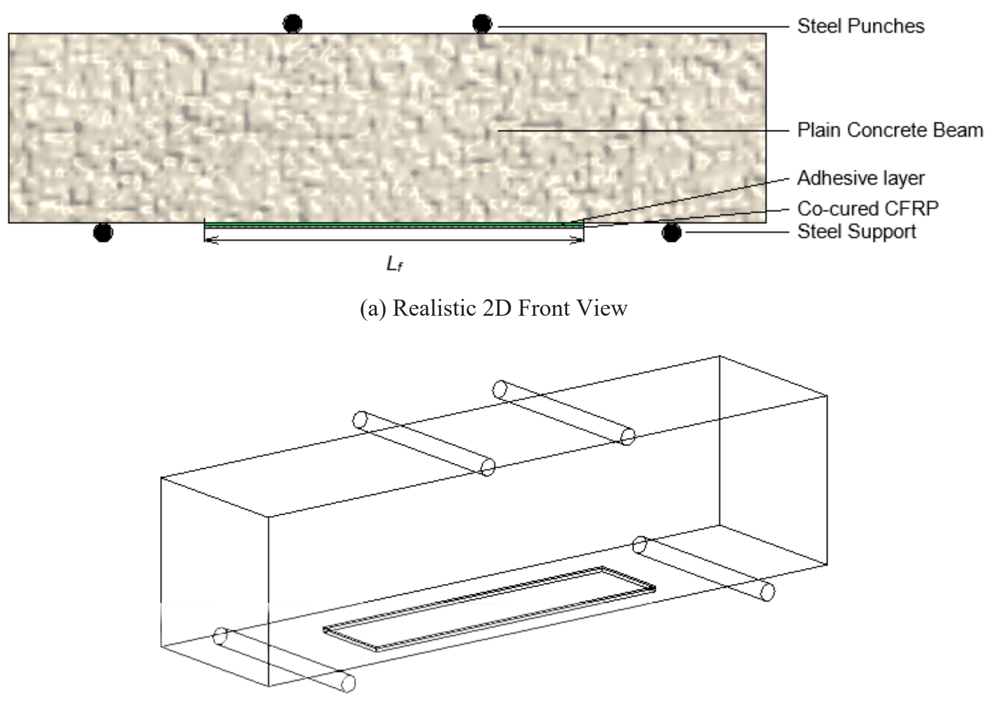

(a) Realistic 2D Front View

(b) Wireframe 3D View

FIGURE 1. Schematic for Four-point bending test setup

TABLE 1. Specimen designation

Specimen Designation	No. of Specimens	c-CFRP Dimensions (L_f x W_f x t_f)	c-CFRP Volume (cm^3)	Normal CFRP Density Fraction, V_f (%)
CTL	3	-	-	-
L100	3	100 x 50 x 2	100	15
L150	3	150 x 50 x 2	150	15
L200	3	200 x 50 x 2	200	15

MATERIAL PREPARATIONS

This section covers the casting of a beam specimen, the concrete mix design, the physical tests, and the curing process. This is followed by preparing the beam for the application of CFRP plates. The co-curing process used in this study is the room-temperature curing of CFRP laminates on steel plates. The chosen method was intentionally designed to balance experimental feasibility with the need to produce co-cured laminates under consistent and controlled conditions. Then, the load-deflection relations were developed from the beam's results from the four-point bending test. The next sub-section is discussed in more detail in this study.

PREPARATION OF CONCRETE BEAM

The mix design for the plain concrete beam refers to Teychenne et al (2010). The grade of concrete is designed for the compression cube strength of 25N /mm^2 (M25). The concrete mixed proportions were intended to achieve strength and workability, using precise ratios of cement, fine and coarse aggregates, and water to ensure realistic structural responses under flexural loads. Plain concrete contains aggregates, a binder, and water. The mix proportion of concrete is presented in Table 2. The targeted slump value for the mix is 10-30 mm to achieve a characteristic compressive cube strength of 25 N/mm^2.

TABLE 2. Proportion of concrete mix M25

Mix Ratio	0.59	1	2.78	3.13
Quantities (kg/m^3)	190	320	890	1000

The overview of the concrete mixing procedure is shown in Figure 1. As per the workability guidelines described in BS EN 12350-2 (2019). The slump value is 19 mm (refer to Figure 2 (a)), which lies between the designated slump value to attain the characteristic compressive cube strength of 25 N/mm^2. The inner surface of the framework used to cast the beam is coated with sufficient grease to help prevent the concrete from sticking to the framework and facilitate the specimen's removal. Then, the concrete is poured into the plastic moulds, where compaction is performed using a poker vibrator, as shown in Figure 2(b). The concrete is left to harden for 24 hours, after which it is removed from the frame and cured in accordance with BS EN 12390-2 (2019). The specimen is then fully immersed in a curing tank for 25 days. Figure 2 (c) shows that beam specimens were taken out and left air-dried for 3 days, as the process of strengthening c-CFRP plates was discussed in Section 2.2.3 later.

Meanwhile, the hardened properties of concrete include density and the compression cube test, which are carried out when the cube is tested at 28 days from the day of casting, based on BS EN 12390-3 (2019). The dry cube density of concrete was 2190 kg/m3, whereas the designated hardened cube dry density was 2210 kg/m^3. The designated compression cube strength for the concrete is 25 N/$mm^{2,}$ whereas the achieved value at 28 days is 26.6 N/mm^2.

PREPARATION OF c-CFRP PLATES

This section describes the preparation of c-CFRP plates. The woven fabric carbon fibre has a thickness of 0.166 mm, Young's modulus (E) of 41595 GPa, and Shear modulus (G_{xy}) of 1063 MPa. Initially, the two fabric layers were made with the application of epoxy resin named Epikote 828 Epoxy Resin with the ratio of epoxy to hardener was 5:2. The fabrication start with the steel plate surface was sprayed with grease (refer Figure 3 (a)) for the easy removal of c-CFRP plates later, and then a layer of epoxy resin was applied as shown in Figure 3 (b). Then, Figures 3(c), (d), and (e) show that the woven fabric carbon fibre was placed over the first layer of epoxy resin, and the same procedure was repeated for the next layer; the final coating of epoxy resin was then applied over the top of CFRP. Figure 3(f) shows that it was left to dry for 24 hours to harden. Figure 4 compares a normal CFRP sheet and a c-CFRP plate. Finally, the c-CFRP were cut to the desired length, noting that the fabrication was done at room temperature.

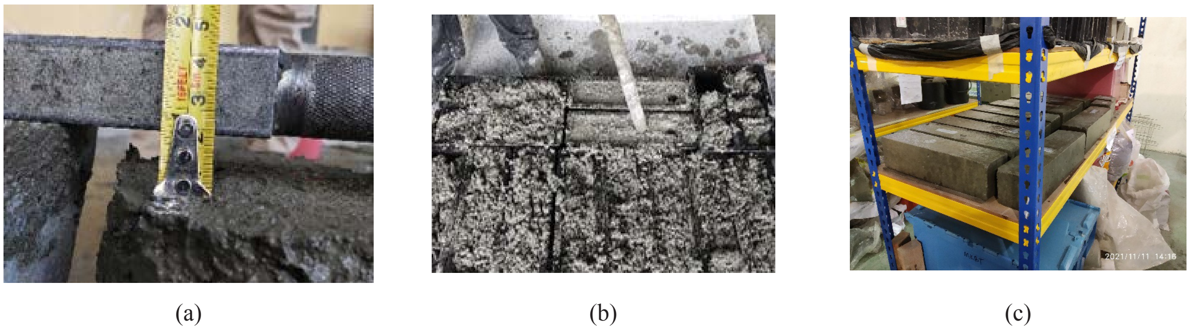

FIGURE 2. Beam concrete process overview

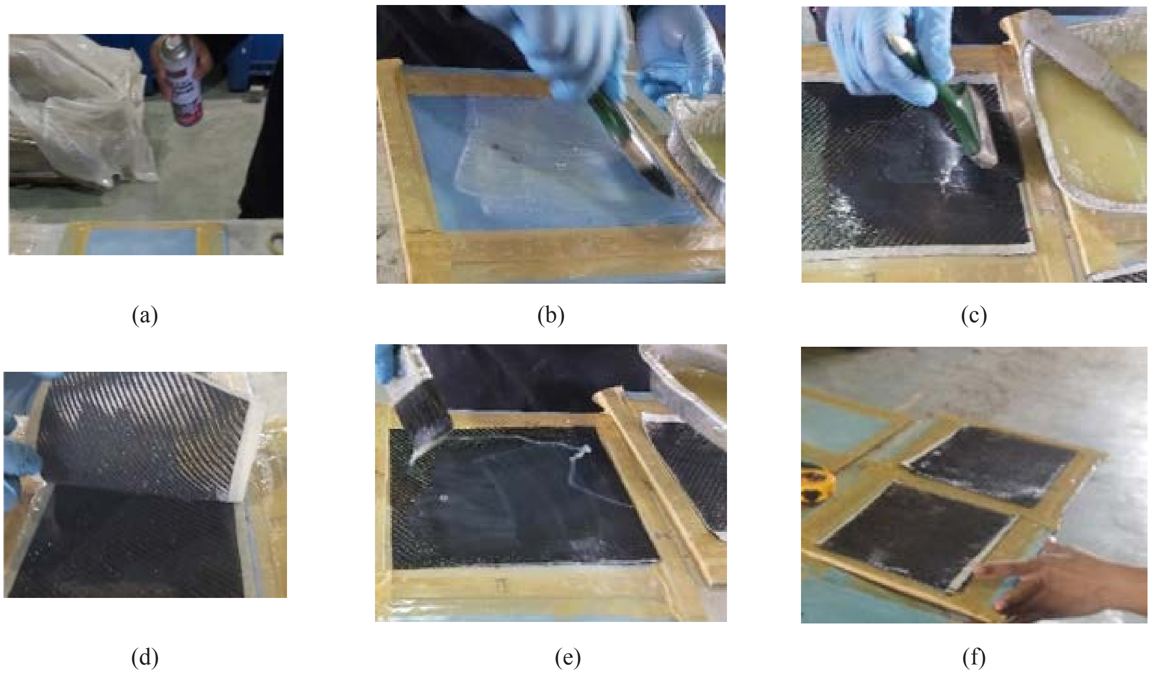

FIGURE 3. c-CFRP fabrications

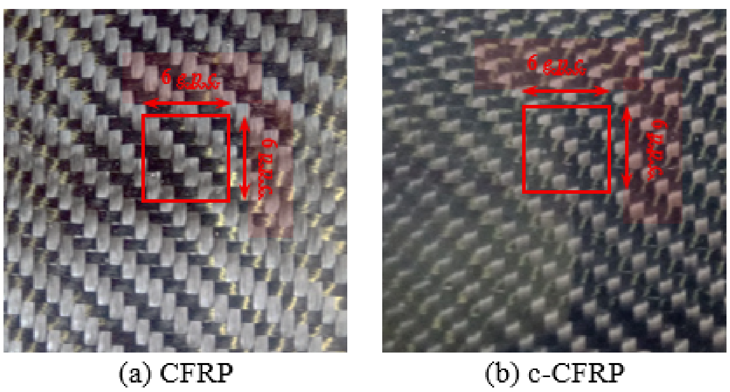

FIGURE 4 Comparison between (a) before and (b) after for c-CFRP fabrications

CONCRETE SURFACE TREATMENT AND APPLICATION OF C-CFRP PLATE

This sub-section guideline and procedure refer to ACI.2R-17 [9]. The specimen's tension face is considered the beam's bonding surface. Figure 5(a) shows the low-speed mode, with a wire brush used to roughen the concrete beam's surface and provide good adhesive bonding with c-CFRP plates. Then, the c-CFRP plate surface was also scraped with a knife parallel to its length, as shown in Figure 5(b). The Sikadur-31 SBA S-02 (SK31) was used as an adhesive layer due to its high viscosity and slow flow, which helps bonded CFRP plates remain over the concrete beam. The SK31 was applied to the concrete beam after cleaning its surface of debris. Then, c-CFRP plates were pushed onto the applied surface of the epoxy resin. Finally, Figure 5(c) shows that all strengthened concrete beams with c-CFRP plates were air-dried for at least 24 hours before flexural testing.

TESTING OF SPECIMENS

The Universal Testing Machine (UTM), with a load cell capacity of 50 kN and a constant crosshead speed of 0.5 mm/min, was used to allow sufficient time for crack propagation and prevent sudden failure in the specimen. The mid-span deflection was measured using the built-in vertical linear displacement sensor, which is installed within the UTM machine. The sampling interval rate was set at 0.5 points per second. A data acquisition system analysed load-deflection data, and the visualisation of cracks and failure modes was performed. The specimen was placed between two supports: one hinged and the other a roller. The loading points are made from steel to ensure zero deformation. The steel roller's diameter and length, as in supports and punches, were measured as 10mm and 120mm, respectively. The camera recorded all the specimens tested during bending. The experimental programme followed BS EN 12390-5 (2019), which specifies that a minimum of three specimens is required to obtain an average flexural strength value.

The purpose of this study was not to perform an extensive statistical analysis, but rather to investigate the fundamental behaviour of plain concrete beams strengthened with c-CFRP plates. However, averaging three specimens occasionally led to large deviations due to inconsistent failure modes in practice, particularly when premature debonding occurred. For this study, premature debonding was defined as a failure mode in which the load–deflection response showed a sudden brittle drop without reaching at least 80% of the peak load capacity typically achieved by specimens of the same group, and the graph indicated a lack of ductile behaviour. In such cases, specimens were excluded to ensure that the representative response reflected the intended strengthening behaviour rather than anomalous premature failure. The tests are conducted on the 28th day of the specimen.

(a) (b) (c)

FIGURE 5. Concrete beam strengthened with c-CFRP plate preparation

(a) (b)

FIGURE 6 Mechanical test set-up

RESULTS & DISCUSSION

This section started with experimental observations, failure modes, and typical load-displacement profiles. Then, the load-displacement curves of length variation were discussed. Finally, the performance of c-CFRP plates of varying lengths was addressed at the end of this section.

FAILURE MODES CONCERNING LOAD-DISPLACEMENT PROFILES

Fifteen beam specimens were tested under four-point bending to evaluate their failure behaviour. Typically, at least two of the three specimens in each group displayed consistent behaviour, and a single representative curve was used for comparison across different plate lengths. Based on visual observation, recorded video and load-deflection behaviour, three distinct modes of failure were identified through observations: flexural failure in unstrengthened concrete beams (F), shear crack propagates from the c-CFRP tip to the point load (ST), and flexural ruptures in concrete following c-CFRP plate delamination (FD), as shown in Figure 7.

Among the tested specimens, all three unstrengthened control beams (CTL) failed in F mode, characterised by mid-span cracking due to the tensile weakness of plain concrete. For specimen series L100, all three beams failed in ST mode, with cracks initiating near the CFRP tip and propagating diagonally toward the load application points, indicating an insufficient c-CFRP length to prevent shear failure. In the L150 series, one beam failed in ST mode, while the remaining two specimens failed in FD mode, indicating partial improvement in flexural resistance. Meanwhile, all beams in the L200 and L250 series failed in FD mode, suggesting that longer c-CFRP plates (≥200 mm) enhance flexural capacity and effectively delay shear-related failure. These findings are summarised in Figure 8, which shows that 53% of the specimens failed in FD mode, followed by 27% in ST and 20% in F mode.

Figure 9 presents the representative load–deflection behaviour and corresponding 3D schematic illustrations of three key failure modes observed during the experimental testing. The selected specimens are CTL, L100, and L250, which reflect the progression in structural performance due to varying c-CFRP plate lengths. It is important to note that the 3D schematic diagrams are not derived from numerical modelling; instead, they were manually developed to visually represent the actual failure patterns observed in the laboratory during physical testing.

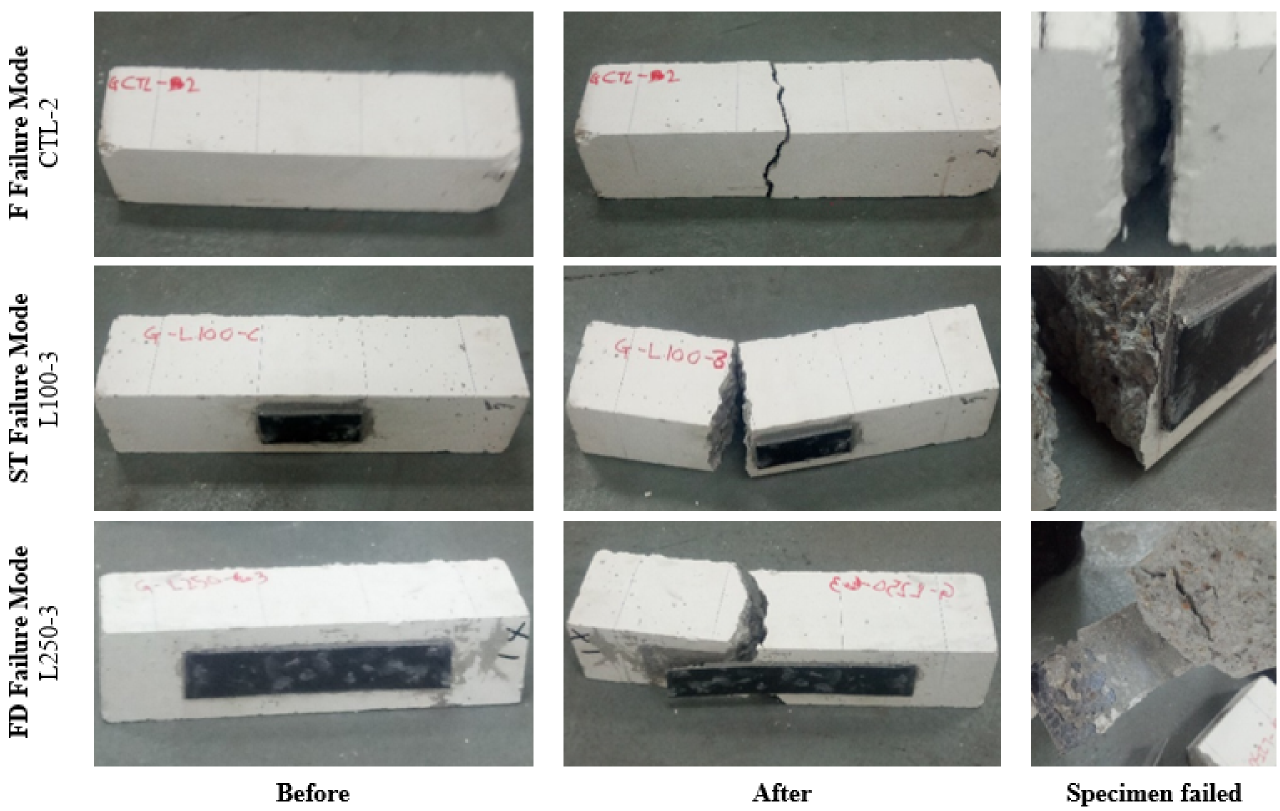

.FIGURE 7. Photographs of Typical Failure Modes

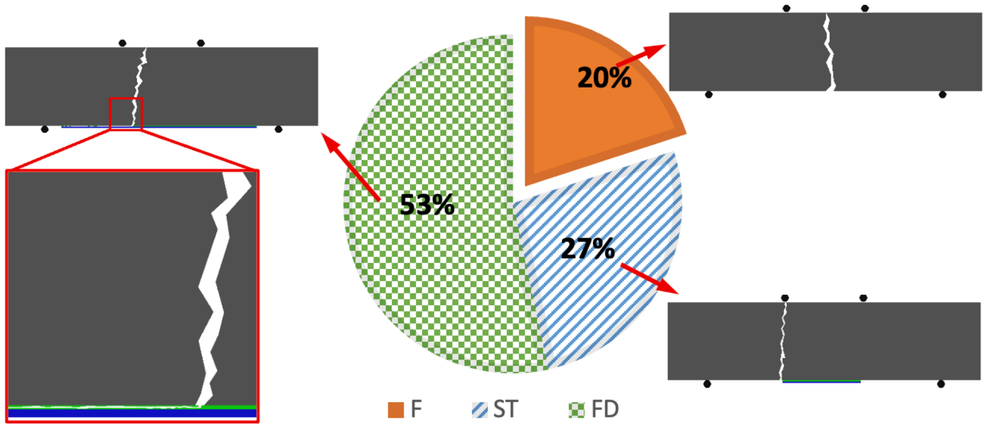

.FIGURE 8. Distribution of Failure Modes Among All Tested Beams

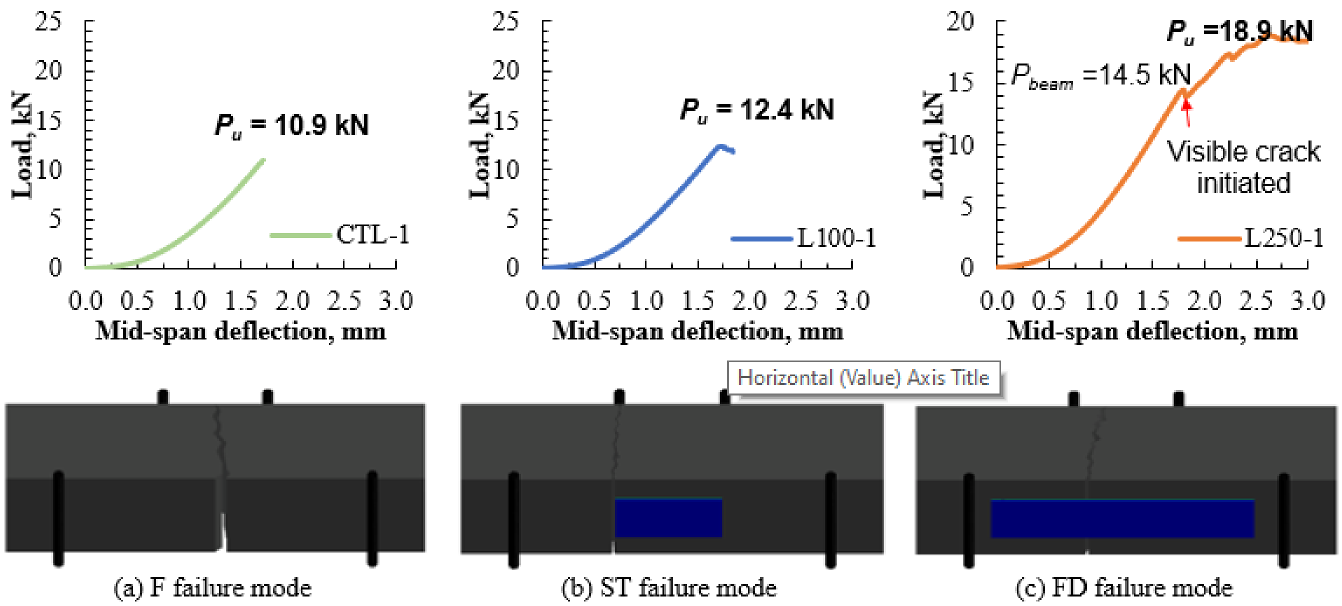

FIGURE 9. Load–deflection curves and corresponding 3D failure representations for three failure modes

The unstrengthened control beam demonstrated typical flexural failure behaviour, as shown in Figure 9 (a). The load–deflection curve shows a modest capacity with an ultimate load, P_u of 10.9 kN and a relatively steep decline after peak load, indicating brittle failure. As shown in the schematic, cracking initiated at the mid-span within the tension zone and propagated vertically upwards due to the plain concrete's limited tensile strength. This phenomenon is consistent with the load-deflection graph, in which the control beam exhibited the lowest load-carrying capacity and stiffness, underscoring its susceptibility to flexural damage. The flexural failure observed in the CTL is characterised by the upward propagation of vertical cracks emanating from the tension zone. No external reinforcement was present to redistribute tensile stresses, leading to a sudden, brittle failure mode.

In the L100 specimen, strengthened with a 100 mm c-CFRP plate, the ultimate load increased slightly to 12.4 kN. However, all specimens in this group failed in the ST mode, characterised by diagonal shear cracks emanating from the tip of the

c-CFRP plate, as shown in Figure 9(b). The load–deflection response, though improved compared to the control, still showed relatively brittle behaviour, and failure occurred via a shear crack mechanism. This was due to local stress concentrations at the abrupt termination of the c-CFRP, which was too short to effectively anchor and transfer tensile forces beyond its bonded region. The resulting failure mode was governed by shear stress concentration at the interface transition between strengthened and unstrengthened regions. The schematic visualises this failure mechanism, which agrees with the physical observations. Although beneficial for mid-span flexure, it did not extend far enough to prevent shear-related cracking beyond the reinforced zone.

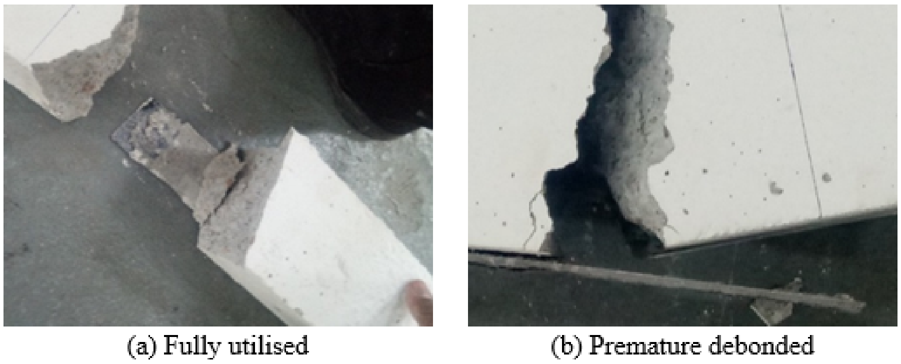

FIGURE 10. Debonding of CFRP from the concrete surface

In contrast, the L250 beam, which was strengthened with a 250 mm c-CFRP plate, achieved a substantially higher ultimate load of 18.9 kN, nearly double that of the control beam. On the other hand, the load at beam failure refers to the load at which the first visible crack appears (detectable by the naked eye) and marks the moment when the c-CFRP begins actively resisting tensile stresses transferred through the beam opening. The load–deflection curve shows an extended deformation range and increased ductility, indicating a more gradual, energy-absorbing failure process. The 3D schematic shows horizontal and inclined cracks concentrated within the CFRP-covered region, along with evidence of delamination between the CFRP plate and the concrete surface. This was not premature debonding, as the CFRP remained effective up to and beyond the maximum load. In the intermediate phase, as the load intensifies, the crack widens and lengthens. The CFRP plate is pivotal in managing crack widths and redistributing stresses, skilfully postponing any imminent catastrophic failure. In the final phase, the beam attains its peak capacity when a critical crack pierces through the CFRP plate or the adhesive connection between the plate and the concrete fails. The typical failure modes for beams reinforced with c-CFRP plates include debonding the c-CFRP plate or crushing concrete within the compression zone. The schematic illustrates the crack patterns under the c-CFRP region, reflecting a well-anchored and efficient reinforcement system that enhanced strength, stiffness, and energy absorption. In contrast, the lengthier c-CFRP plate on the concrete beam may experience premature debonding failure. Figure 10 shows the comparison between fully utilised c-CFRP and premature debonded failure. It can be observed that fully utilised areas were indicated based on the concrete substrate attached to c-CFRP, while some adhesives were found attached to the concrete beam. No concrete debris was attached to the c-CFRP when the prematurely debonded areas were seen. The excessive length of the c-CFRP plate likely led to stress concentrations or early debonding at the concrete and c-CFRP interface, diminishing its overall effectiveness.

LOAD-DISPLACEMENT CURVES OF C-CFRP LENGTH VARIATION

Figure 11 illustrates the representative load–deflection curves for the control beam (CTL) and beams strengthened with c-CFRP plates of varying lengths: 100 mm, 150 mm, 200 mm, and 250 mm. Each curve represents a single beam from its respective group, carefully selected based on consistency. Specifically, two out of three specimens in each group showed comparable responses. Any curves displaying premature debonding or atypical failure were excluded from this comparison to maintain clarity and focus on the most representative structural behaviours. From Figure 10, it is evident that the ultimate load and corresponding deflection increase with increasing plate length, indicating enhanced load-carrying capacity and energy absorption.

The control beam (CTL) without c-CFRP reinforcement exhibited the lowest load capacity and stiffness. Its behaviour was distinctly brittle, failing in pure flexure due to the limited tensile strength of unreinforced concrete. The beam's initial stiffness and ultimate load capacity increased upon strengthening with a 100 mm c-CFRP plate (L100). However, the gain was modest, and failure occurred due to shear cracking at the tip of the CFRP plate, resulting from an insufficient bonded length to fully develop flexural enhancement or to distribute stresses effectively beyond the reinforced zone.

Notably, for specimens L150, L200, and L250, the curves exhibit a distinct peak following an initial linear region of constant stiffness. This peak marks the onset of visible cracking, observed directly during testing, and indicates the transition from uncracked elastic behaviour to the cracked flexural response. Despite differences in ultimate load, these three specimens show similar initial stiffness, suggesting that early-stage flexural rigidity is governed primarily by the strengthened beam's concrete section and effective bond development, rather than the plate length alone.

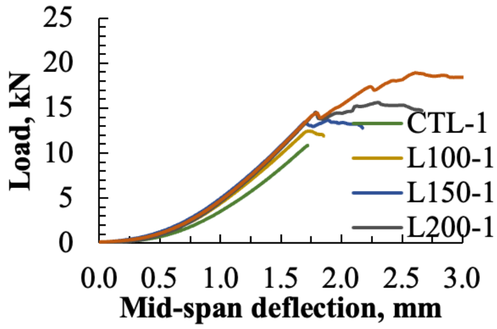

FIGURE 11. Typical loaddeflection curves for control and c-CFRP-strengthened beams with varying plate lengths

TABLE 3. Summary of strengthened plain concrete beam performances

Specimen	No.	Failure Mode	P_{beam} (kN)	P_u (kN)	Average P_u (kN)	δ_u (mm)	Average δ_u (mm)	EA (kN·mm)	k kN/mm)
CTL	1	F	-	10.89	10.83	1.72	1.71	6.18	6.34
	2	F	-	10.95	± 0.15	1.74	± 0.04		
	3	F	-	10.66		1.67			
L100	1	ST	-	12.42	12.46	1.72	1.72	8.94	7.21
	2	ST	-	12.36	± 0.13	1.72	± 0.01		
	3	ST	-	12.61		1.70			
L150	1	FD	13.47	13.68	13.68	1.88	1.92	14.28	7.92
	2	FD	13.64	13.67	± 0.01	1.95	± 0.05		
	3*	ST	-	13.25		1.77			
L200	1	FD	14.46	15.61	15.59	2.31	2.20	21.66	8.04
	2	FD	14.37	15.57	± 0.02	2.10	± 0.15		
	3*	FD	-	13.92		1.82			
L250	1	FD	14.52	18.94	18.29	2.61	2.32	31.69	8.03
	2	FD	14.41	17.64	± 0.92	2.42	± 0.35		
	3*	FD	-	14.21		1.93			

Notes: '*' were excluded from averages and standard deviation

The L250 specimen exhibited the highest overall performance, reaching a peak load of approximately 18.9 kN and a stable, extended post-peak deflection range. This indicates excellent energy absorption and delayed failure, attributed to the optimal distribution of tensile stresses and improved anchorage provided by the longer c-CFRP plate. The sustained load capacity beyond initial cracking confirms that longer plates contribute to peak strength and enhanced post-crack ductility and energy absorption.

PERFORMANCE OF C-CFRP LENGTHS ON CONCRETE BEAM

Table 3 summarises the performance of strengthened plain concrete beams, organised by specimen type and corresponding failure modes. The load at beam failure, P_{beams} refers to the load at which the first visible crack appears (detectable by the naked eye) and marks when the c-CFRP begins to resist tensile stresses transferred through the beam opening actively. Then, the ultimate load, P_u is the maximum load sustained by the beam before global failure. The deflection at peak load, δ_u corresponds to the mid-span displacement at ultimate load, indicating the beam's deformability. For each group, the ultimate load and deflection at peak are reported along with their average values and standard deviations, based on three specimens tested in line with BS EN 12390-5:2019. It should be noted that some results marked with an asterisk ('*') were excluded from the averages and standard deviations, as these specimens failed by premature debonding or exhibited a failure mode inconsistent with the intended flexural behaviour.

Meanwhile, Energy Absorption (*EA*), quantified as the area under the load-deflection curve up to complete separation, reflects the beam's capacity to absorb mechanical energy and resist fracture, indicating ductile behaviour to resist transferred stresses. Lastly, the secant stiffness (*k*) is derived from the slope of the initial linear portion of the load–deflection curve and indicates the elastic stiffness before significant cracking. The energy absorption and secant stiffness values were not averaged but derived from the most representative load–deflection curve previously shown in Figure 11, ensuring that these parameters reflected a consistent and realistic mechanical response.

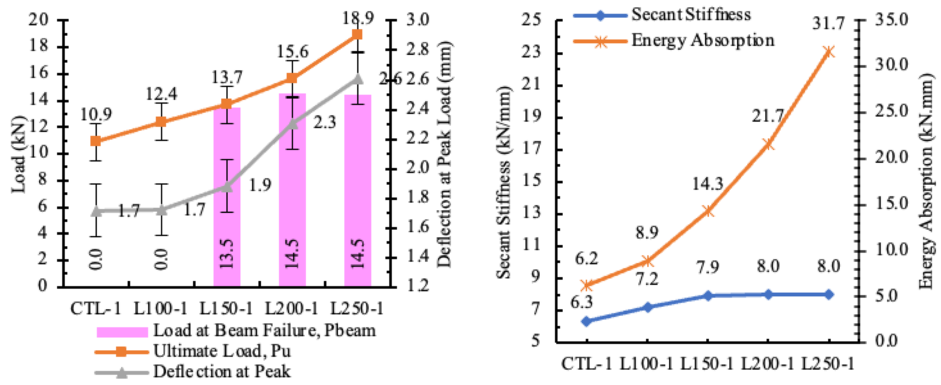

(a) (b)

FIGURE 12. The performance of the c-CFRP plates

Figure 12 shows the performance of c-CFRP as a strengthened plain concrete beam exhibited from the first specimen for each specimen designation. From Figure 12, the CTL specimen, which failed in pure flexure, showed the lowest values in nearly all categories: an ultimate load of 10.89 kN, a deflection at peak of 1.72 mm, energy absorption of 6.18 kN·mm, and a secant stiffness of 6.34 kN/mm. The L100 beam, strengthened with a 100 mm c-CFRP plate, showed a modest improvement in load bearing and stiffness, with a slightly higher ultimate load of 12.42 kN and energy absorption of 8.94 kN·mm, but retained the same deflection as CTL, indicating limited ductility gain. However, significant performance enhancements are evident in beams with longer c-CFRP plates. L150 and L200 exhibited progressive increases in ultimate load (13.68 kN and 15.61 kN, respectively), energy absorption (14.28 kN·mm and 21.66 kN·mm), and peak deflection, reflecting improved crack resistance and ductility. Notably, the L250 beam achieved the highest values across all key indicators: 18.94 kN ultimate load, 2.61 mm peak deflection, and 31.69 kN·mm energy absorption, confirming its superior load resistance and energy dissipation capacity. Interestingly, the secant stiffness values for L150, L200, and L250 were comparable (around 8.0 kN/mm), suggesting that the initial flexural rigidity stabilised beyond a certain CFRP length.

It is interesting to focus on the load at beam failure and the ultimate load. The control beam reached an ultimate load of 10.89 kN, representing the baseline strength of unstrengthened concrete. When strengthened, the load at first shows visible cracking, P_{beam} increased from 10.89 kN in the control beam to 13.47 kN in L150, 14.46 kN in L200 and 14.52 kN in L250, confirming that c-CFRP enhanced the beams' initial cracking resistance. This improvement demonstrates that even though c-CFRP is primarily engaged after cracking, its presence contributes positively at the onset of cracking once a sufficient bonded length is provided. Beyond crack initiation, the ultimate load (P_u) further illustrates the strengthening effect. As c-CFRP resisted crack propagation and delayed failure, the ultimate load increased progressively with plate length: 13.68 kN (L150), 15.59 kN (L200), and 18.29 kN (L250). Longer bonded lengths allowed for more effective stress redistribution and higher load-carrying capacity. The ductile post-peak behaviour observed in L150, L200 and L250 beams reflected gradual stress transfer until one side of the plate debonded, whereas shorter plates provided limited enhancement. Meanwhile, specimens that failed by premature debonding or ST failure mode did not register meaningful P_{beam}, as cracks developed suddenly without a significant contribution from the strengthening system. These cases highlight the importance of sufficient bonded length to ensure proper engagement of c-CFRP and prevent brittle, non-ductile failures.

Furthermore, the deflection at peak load provides essential insight into the strengthened beams' ductility, complementing the increases observed in ultimate load. As shown in Figure 12, the CTL reached only about 1.7 mm of deflection at peak, reflecting brittle behaviour typical of plain concrete. With increasing c-CFRP plate length, the peak deflection also increased, rising to 1.9 mm (L150), 2.3 mm (L200), and 2.6 mm (L250). This trend demonstrates that longer c-CFRP plates not only increased load capacity but also enhanced the beams' ability to undergo larger deformations before failure, indicating a transition from brittle to more ductile behaviour.

The results in Figure 12(b) clearly show that energy absorption plays a much greater role in differentiating the performance of strengthened beams than stiffness does. While the secant stiffness remained nearly constant across all specimens, fluctuating slightly around 6.3–8.0 kN/mm, the energy absorption increased dramatically with c-CFRP plate length, from 6.2 kN·mm for the control beam to 31.7 kN·mm for L250. This represents more than a fivefold improvement, demonstrating that longer c-CFRP plates enhanced load capacity and allowed the beams to dissipate significantly more energy before failure. Such an increase in energy absorption is critical, as it reflects the beams' ability to resist cracking, sustain higher deformation, and undergo progressive debonding rather than brittle failure. In structural applications, this ductile energy-dissipating behaviour is far more valuable than marginal gains in stiffness, since it directly contributes to resilience, toughness, and safety under service and extreme loading conditions.

Moreover, the scope of this research was limited to comparing plain concrete beams with those strengthened by c-CFRP plates to establish the baseline behaviour of this strengthening method. Traditional wet lay-up CFRP systems were not repeated experimentally, as their performance has already been extensively documented in the open literature. The experimental results of this study reveal that c-CFRP plates significantly enhance the flexural performance of plain concrete beams, with the optimum performance observed for plate lengths between 200 mm and 250 mm. This is consistent with the findings by Zhang et al. (2021), who investigated externally bonded CFRP sheets on plain concrete beams and reported improvements in ultimate load and deformation capacity. However, unlike their study, which primarily used wet-lay-up CFRP sheets, the c-CFRP plates used in the current study provided greater consistency in bond performance and surface uniformity, resulting in more stable crack propagation and delayed delamination. Eliminating resin-rich zones in co-cured systems likely contributed to this enhanced behaviour.

Similarly, Al-Rousan et al. (2018) demonstrated that increased CFRP length contributes to higher ductility and energy absorption. However, their dry-saturated FRP systems resulted in early bond degradation and more varied failure modes across specimens. In contrast, the co-cured system employed here showed improved control over interface performance and enabled more reliable prediction of failure mechanisms. While Al-Rousan et al. (2018) noted a trade-off between CFRP length and interfacial stresses, the current study found that a 200 mm to 250 mm plate balanced stress distribution and bond effectiveness, reducing the likelihood of sudden delamination.

Omar et al. (2022) explored the use of woven kenaf fibre FRP (KFRP) for strengthening plain concrete beams and reported that the fibre configuration and bonding area directly influenced failure patterns. Although natural fibres like kenaf showed potential for sustainable retrofitting, their performance was limited by lower tensile strength and greater susceptibility to interfacial debonding. The current study reinforces this conclusion by demonstrating that synthetic c-CFRP, when properly applied and co-cured, yields higher load capacities (up to 18.94 kN for L250) and energy absorption (up to 31.69 kN·mm), outperforming natural fibre systems in both stiffness and crack resistance.

Regarding failure behaviour, Azhar et al. (2025) identified the importance of CFRP anchorage and plate length in reducing peel and shear stresses at the ends of the bonded region. Their findings emphasised that insufficient bonded length or poor surface preparation often leads to premature shear or combined tension–shear failures. While such combined failures were also observed in shorter plates (L100) in the current study, no premature debonding was found in longer plates (L200 and L250), which demonstrated improved crack control and load transfer. This confirms the effectiveness of the co-cured interface in mitigating localised stress concentrations and allowing gradual crack propagation rather than sudden detachment.

Lastly, the failure mode classification in the present study (F, ST, and FD) aligns well with failure typologies observed in past literature, though with some differences in terminology and interpretation (Al-Rousan et al. 2018; Azhar et al. 2025; Omar et al. 2022). In contrast to ST failures identified in this study as shear cracks initiating at the tip of c-CFRP plates, many previous studies described similar occurrences as "shear-flexural" or "debonding-initiated" failures (Al-Rousan et al. 2018; Huang et al. 2015b; Maulana et al. 2022; Omar et al. 2022).

CONCLUSIONS

This study evaluated the effect of the length variation of externally bonded c-CFRP plates on the flexural behaviour of plain concrete beams. A total of 15 specimens (five sets, three per group) were tested under four-point bending. The results demonstrated that c-CFRP strengthening significantly improves ultimate load, stiffness, and energy absorption. The control beam (CTL) recorded the lowest ultimate load (10.89 kN), energy absorption (6.18 kN·mm), and stiffness (6.34 kN/mm), failing in brittle flexure. The L100 beam improved only marginally (12.42 kN, 8.94 kN·mm), failing due to shear cracking at the tip of the CFRP plate. Meanwhile, L200 and L250 specimens achieved ultimate loads of 15.61 kN and 18.94 kN, and energy absorptions of 21.66 kN·mm and 31.69 kN·mm, respectively, demonstrating superior ductility and crack resistance. All strengthened specimens showed similar initial stiffness (~8.0 kN/mm), indicating adequate bonding during elastic behaviour. The experimental methodology was carefully designed to isolate the effect of c-CFRP length, using consistent materials, casting procedures, and curing regimes. Based on consistency in behaviour, selecting one representative specimen per group helped eliminate premature debonding anomalies, thereby reinforcing the study's internal validity. Significantly, the onset of cracking (load at beam failure) shifted higher with increasing plate length (e.g., 13.47 kN for L150, 14.52 kN for L200), indicating that the c-CFRP effectively delayed crack initiation. These results confirm that a plate length of 200 mm or greater provides optimal balance between strength, ductility, and bonding effectiveness. Future research should investigate adhesive characterisation, multiple CFRP layers, and long-term durability under environmental exposures and cyclic loading, and test on a reinforced concrete beam to expand the reliability and scope of c-CFRP strengthening techniques in real-world applications.

ACKNOWLEDGEMENT

This research was funded by a grant from Universiti Sains Malaysia (Short-Term Grant with Project No. R501-LR-RND002-0000001166-0000).

DECLARATION OF COMPETING INTEREST

None.

REFERENCES

Al-Rousan, R. Z., Al-Hassan, M. A. & Al-Shuqari, E. A. 2018. Behavior of plain concrete beams with DSSF strengthened in flexure with anchored CFRP sheets: Effects of DSSF content on the bonding length of CFRP sheets. *Case Studies in Construction Materials* 9: e00195. https://doi.org/10.1016/j.cscm.2018.e00195

Azhar, S., Sugiman, S., Omar, Z. & Ahmad, H. 2025. Experimental investigations of strengthened beam with co-cured carbon FRP and mussel shell-modified epoxy. *Ain Shams Engineering Journal* 16(10): 103563. https://doi.org/10.1016/j.asej.2025.103563

BS EN 12350-2:2019. 2019. *Testing Fresh Concrete — Part 2: Slump Test*. British Standards Institution.

BS EN 12390-2:2019. 2019. *Testing Hardened Concrete — Part 2: Making and Curing Specimens for Strength Tests*. British Standards Institution.

BS EN 12390-3:2019. 2019. *Testing Hardened Concrete — Part 3: Compressive Strength of Test Specimens*. British Standards Institution.

BS EN 12390-5:2019. 2019. *Testing Hardened Concrete — Part 5: Flexural Strength of Test Specimens*. British Standards Institution.

Ferreira, M. V. F., Neves, A. C. C., Oliveira, C. G. de, Lopes, F. P. D., Margem, F. M., Vieira, C. M. F. & Monteiro, S. N. 2017. Thermogravimetric characterization of polyester matrix composites reinforced with eucalyptus fibers. *Journal of Materials Research and Technology* 6(4): 396–400. https://doi.org/10.1016/j.jmrt.2017.09.002

Gao, P., Gu, X. & Mosallam, A. S. 2016. Flexural behavior of preloaded reinforced concrete beams strengthened by prestressed CFRP laminates. *Composite Structures* 157: 33–50. https://doi.org/10.1016/j.compstruct.2016.08.013

Huang, X., Wang, J., Zhang, F., Niu, S. & Ding, J. 2015a. An experimental investigation on the failure behavior of a notched concrete beam strengthened with carbon fiber-reinforced polymer. *International Journal of Polymer Science* 2015: 729320. https://doi.org/10.1155/2015/729320

Huang, X., Wang, J., Zhang, F., Niu, S. S. & Ding, J. 2015b. An experimental investigation on the failure behavior of a notched concrete beam strengthened with carbon fiber-reinforced polymer. *International Journal of Polymer Science* 2015: 729320. https://doi.org/10.1155/2015/729320

Kang, T. H. K., Howell, J., Kim, S. & Lee, D. J. 2012. A state-of-the-art review on debonding failures of FRP laminates externally adhered to concrete. *International Journal of Concrete Structures and Materials* 6(2): 123–134. https://doi.org/10.1007/s40069-012-0012-1

Kumar, P., Bishnoi, S. & Bhattacharjee, B. 2020. Influence of CFRP strand sheet on flexural strengthening of reinforced concrete beam. *Journal of Advanced Concrete Technology* 18(12): 778–793. https://doi.org/10.3151/JACT.18.778

Liao, J., Li, H., Zheng, Y., Geng, L., Zhuge, Y. & Zeng, J. 2026. Flexural performance of CFRP grid-reinforced ultra-high performance concrete (UHPC) plates under cyclic incremental loading. *Engineering Structures* 351: 122005. https://doi.org/10.1016/j.engstruct.2025.122005

Maulana, M. R., Sugiman, S., Ahmad, H., Jaini, Z. M. & Mansor, H. 2022. XFEM modelling and experimental observations of foam concrete beam externally bonded with KFRP sheet. *Latin American*

Journal of Solids and Structures 19(6). https://doi.org/10.1590/1679-78257205

Motsch-Eichmann, N., Rieger, F., Rief, T. & Hausmann, J. 2021. Experimental investigation of modified co-curing process for carbon fiber/epoxy-laminates. *Journal of Micromechanics and Molecular Physics* 6(3): 1–12. https://doi.org/10.1142/S2424913021430013

Muravsky, L., Nazarchuk, Z., Kuts, O., Ivanytskyi, Y. & Sharabura, O. 2025. Detecting of interfacial defects in CFRP–concrete bonded joints using dynamic speckle patterns of excited surface. *NDT & E International* 156: 103480. https://doi.org/10.1016/j.ndteint.2025.103480

Nadzri, S. N. Z. A., Sultan, M. T. H., Shah, A. U. M., Safri, S. N. A. & Basri, A. A. 2020. A review on the kenaf/glass hybrid composites with limitations on mechanical and low velocity impact properties. *Polymers* 12(6): 1285. https://doi.org/10.3390/POLYM12061285

Obaidat, Y. T., Barham, W. S., Shehadeh, A. B. & Obeidat, R. B. 2026. Repair of heat-damaged RC flat slabs using a hybrid CFRP rope–sheet technique. *Results in Engineering* 29: 109271. https://doi.org/10.1016/j.rineng.2026.109271

Omar, Z., Sugiman, S., Yussof, M. M. & Ahmad, H. 2022. The effects of woven fabric kenaf FRP plates flexural strengthened on plain concrete beam under a four-point bending test. *Case Studies in Construction Materials* 17: e01503. https://doi.org/10.1016/j.cscm.2022.e01503

Quan, D., Farooq, U., Zhao, G., Dransfeld, C. & Alderliesten, R. 2022. Co-cured carbon fibre/epoxy composite joints by advanced thermoplastic films with excellent structural integrity and thermal resistance. *International Journal of Adhesion and Adhesives* 118: 103247. https://doi.org/10.1016/j.ijadhadh.2022.103247

Quan, D., Zhao, G., Scarselli, G. & Alderliesten, R. 2022. Co-curing bonding of carbon fibre/epoxy composite joints with excellent structure integrity using carbon fibre/PEEK tapes. *Composites Science and Technology* 227: 109567. https://doi.org/10.1016/j.compscitech.2022.109567

Shrivastava, S. & Tiwari, A. 2018. Strengthening of beams using glass fiber reinforced polymer (GFRP) laminate. *International Journal of Engineering Development and Research* 6(3): 231–239.

Tang, Z., Li, W., Tam, V. W. Y., & Yan, L. (2020), Mechanical performance of CFRP-confined sustainable geopolymeric recycled concrete under axial compression. Engineering Structures, 224(111246). https://doi.org/https://doi.org/10.1016/j.engstruct.2020.111246

Teychenne, D. C., Franklin, R. E. & Erntroy, H. C. 2010. *Design of Normal Concrete Mixes*. Building Research Establishment Ltd.

Tiwary, A. K., Singh, S., Kumar, R., Sharma, K., Chohan, J. S., Sharma, S., Singh, J., Kumar, J. & Deifalla, A. F. 2022. Comparative study on the behavior of reinforced concrete beam retrofitted with CFRP strengthening techniques. *Polymers* 14(19): 4024. https://doi.org/10.3390/polym14194024

Vinh, T. X., Hieu, N. T. & Dat, P. X. 2022. Experimental study on flexural behavior of reinforced concrete beams strengthened with CFRP sheets under sustaining load. *Lecture Notes in Networks and Systems* 366: 108–113. https://doi.org/10.59382/pro.intl.con-ibst.2023.ses1-9

Yang, J., Johansson, M., Al-Emrani, M. & Haghani, R. 2021. Innovative flexural strengthening of RC beams using self-anchored prestressed CFRP plates: Experimental and numerical investigations. *Engineering Structures* 243: 112687. https://doi.org/10.1016/j.engstruct.2021.112687

Yazdani, N., Aljaafreh, T. & Beneberu, E. 2020. Concrete beam flexural strengthening with anchored pre-saturated CFRP laminates. *Composite Structures* 235: 111733. https://doi.org/10.1016/j.compstruct.2019.111733

Younas, H., Yu, J. & Leung, C. K. Y. 2026. Enhancing bond performance of near surface mounted CFRP in high-strength strain-hardening cementitious composites (SHCC) through surface treatment. *Construction and Building Materials* 514: 145534. https://doi.org/10.1016/j.conbuildmat.2026.145534

Zhang, S. S., Ke, Y., Smith, S. T., Zhu, H. P. & Wang, Z. L. 2021. Effect of FRP U-jackets on the behaviour of RC beams strengthened in flexure with NSM CFRP strips. *Composite Structures* 256: 113095. https://doi.org/10.1016/j.compstruct.2020.113095

Zhou, H., Yi, C., Yang, Y., Ou, Y. & Wang, N. 2025. Bond behavior of CFRP-concrete bonded joints with randomly distributed defects: Experimental and numerical studies. *Composite Structures* 369: 119317. https://doi.org/10.1016/j.compstruct.2025.119317